SAND99-8217
Unlimited Release
Printed February 1999

The Influence of Feature Sidewall Tolerance on Minimum Absorber Thickness for LIGA X-Ray Masks

S. K. Griffiths, J. M. Hruby and A. Ting
Sandia National Laboratories, Livermore, California 94551-0969

ABSTRACT

Minimizing mask absorber thickness is an important practical concern in producing very small features by the LIGA process. To assist in this minimization, we have developed coupled numerical models describing both the exposure and development of a thick PMMA resist. The exposure model addresses multi-wavelength, one-dimensional x-ray transmission through multiple beam filters, through the mask substrate and absorber, and the subsequent attenuation and photon absorption in the PMMA resist. The development model describes one-dimensional dissolution of a feature and its sidewalls, taking into account the variation in absorbed dose through the PMMA thickness. These exposure and development models are coupled in a single interactive code, permitting the automated adjustment of mask absorber thickness to yield a prescribed sidewall taper or dissolution distance. We have used this tool to compute the minimum required absorber thickness yielding a prescribed sidewall tolerance for exposures performed at the ALS, SSRL and NSLS synchrotron sources. Results are presented as a function of the absorbed dose for a range of the prescribed sidewall tolerance, feature size, PMMA thickness, mask substrate thickness and the development temperature.

INTRODUCTION

As LIGA becomes more widely established, device designs and performance requirements will increasingly demand the full potential of this new manufacturing technology.[1,2] Relative tolerances on mating piece parts such as splines, bearings, shafts and gear teeth will need to approach those of the highest quality conventional machining and grinding methods. The standards for these conventional methods, developed over many decades, extend to roughly one part in 10,000 for dimensional tolerances, run-out and taper. For LIGA this translates to a variance of only 0.1 μm over a feature height or lateral dimension of one millimeter. Similarly, the range of feature sizes on a single part produced by the best conventional methods spans between two and three orders of magnitude. Again for LIGA this translates to 1 μm details on features of size between 100 μm and one millimeter.

A great many factors influence the overall precision of a finished LIGA part. Vertically tapered LIGA molds may result directly from synchrotron beam divergence, x-ray scattering and tapered openings in the mask absorber.[3,4] Mask tolerances clearly play an important role here. Beyond this, however, PMMA has a coefficient of thermal expansion of nearly 10^{-4} C^{-1}, so a difference between the exposure and plating temperatures of just over one degree Celsius will yield a dimensional shift of one part in 10,000. Variations in water content of the PMMA between exposure and plating may lead to similar or even larger dimensional inaccuracies. Finally, stresses induced as metal is deposited during electrodeposition may distort an otherwise good LIGA mold. This can also lead to overall dimensional errors but will primarily introduce a taper through the height of the finished metal piece.

Another important source of through-thickness taper in LIGA molds lies in the development process.[5,6] As features in unmasked regions on the surface of the mold begin to develop, the newly formed sidewalls of each evolving feature are also contacted by the developer. Although doses in the masked regions are much smaller than those in the regions intended for exposure, development rates at low doses are not negligible when small tolerances are a concern. While in contact with the developer, these sidewalls slowly recede laterally from the feature into masked regions of the PMMA. This lateral development begins only as the feature opens, so those sidewall surfaces closest to the mold top (and bottom for freestanding development) are developed for a longer period than those deeper in the PMMA. The consequence of this progressive formation and development of feature sidewalls is tapered mold cavities having greater lateral extent at the top (and possibly bottom) of the mold. This is illustrated in Fig. 1. The extent and profile of this taper depend on the doses in the masked and unmasked regions, the dose variation through the PMMA thickness, and on the relative dissolution rates associated with these doses. However, in a simplified view, sidewall taper is merely the ratio of the low-dose development rate in masked regions of the PMMA surface and the average development rate in unmasked regions over the entire mold thickness. As such, increasing the thickness of the mask absorber should always reduce sidewall taper.

Minimum feature size is likewise affected by a number of factors. Developing and electroplating small features having aspect ratios much above twenty are extremely difficult since diffusion-limited transport rates yield dissolution and metal deposition rates that are very small.[7,8] As a result, the

ratio of the minimum feature size to the part thickness is now limited to about one part in twenty, well below that of conventional manufacturing methods. A more subtle constraint on minimum feature size is the maximum aspect ratio of the mask. Using photoresists to form the gold mask, this aspect ratio typically cannot exceed about six. By making an intermediate LIGA mask, this maximum aspect ratio can be extended to about ten. The smallest feature size that can be produced by LIGA is therefore limited to be larger than at least 10% of the minimum absorber thickness that will provide acceptable x-ray attenuation during the exposure. Minimizing absorber thickness is thus critical to producing very small LIGA features.

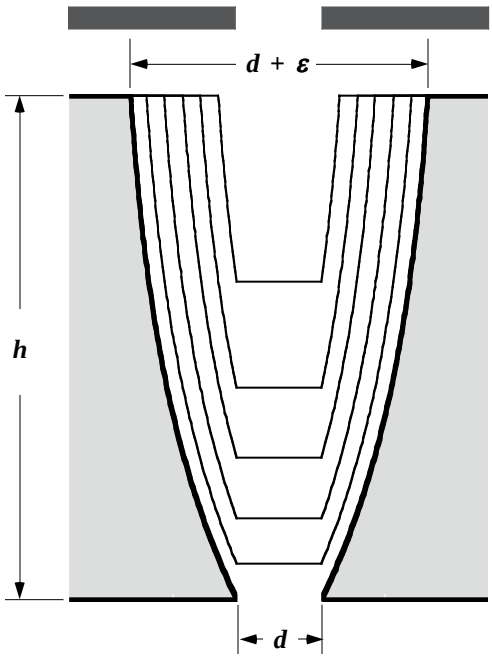

Figure 1. Schematic of a developing LIGA feature. Heavy bars at top indicate gold absorbers on the LIGA mask. The development rate in the unmasked region is initially large, yielding little sidewall dissolution and a nearly straight sidewall profile. As the feature develops into the PMMA, unmasked development rates fall due to the lower absorbed dose and due to diffusion transport limitations. This slowing development rate in the unmasked region produces a roughly parabolic sidewall profile. Lateral development rates in the masked regions shown here are greatly exaggerated to reveal the sidewall profile. Actual sidewall taper is usually a micron or less. Note that the true sidewall taper is given by $\varepsilon/2h$; here we also refer to ε/h as sidewall taper.

From the above discussions, we see that sidewall taper, minimum feature size, dose, development time and absorber thickness are all inherently linked in the LIGA process. Increasing the absorber thickness reduces sidewall taper, but this also increases the minimum possible feature size. Thus to successfully produce very small features having small dimensional tolerances, the thickness of the mask absorber and synchrotron beam filters, the exposure time and the development conditions must all be optimized together.

To help understand the interactions between these many parameters and their effect on sidewall taper, we have developed a numerical model describing both the exposure and development portions of the LIGA process. The one-dimensional exposure model computes the local absorbed dose in both the masked and unmasked regions through the PMMA thickness. This model additionally contains algorithms to automatically adjust exposure time, beam filter thickness and mask absorber thickness so as to yield prescribed doses at both the top and bottom surfaces of the PMMA, as well as a prescribed maximum dose in masked regions under the absorber. The development model, based in part on development rate measurements performed at Sandia, takes into account the local dose,

initial PMMA molecular weight, development temperature and kinetics of the development rate, and the transport of PMMA fragments between the dissolution surface and the open top of the mold. Combined into a single user-friendly code, LEX-D, these two models provide a numerical means for optimizing the mask absorber thickness, beam filter thickness and exposure time, subject to a constraint on the allowable sidewall taper.

NUMERICAL MODEL

The exposure portion of our model describes one-dimensional, multi-wavelength x-ray transmission through an arbitrary set of filters, transmission through the mask absorber and substrate, and the subsequent profile of photon absorption through the thickness of the PMMA target. These transmission and absorption processes are modeled using wavelength-dependent transmission and absorption cross-sections. Scattering is included only as effective forward and backward Compton scattering along the main direction of beam propagation. Fluorescence and other sources of secondary radiation are not yet considered. Under these restrictions, the attenuation of beam power is described by

$$p_{o,k} = p_{i,k}\, e^{-\rho \sigma_{t,k} l} \tag{1}$$

where $p_{i,k}$ is the incident beam power (per eV) at some photon energy E_k, $p_{o,k}$ is similarly the transmitted power, ρ is the material density, $\sigma_{t,k}$ is the transmission cross-section of the material at the photon energy E_k, and l is the thickness of the filter or absorber. Thus the remaining power at any wavelength after any set of filters can be computed by sequential analysis, each time using the transmitted power from the previous filter as the incident power for the next. The mask absorber and substrate can be treated in the same manner. The incident power on the first filter is simply the synchrotron output, properly adjusted to account for the beam length. Synchrotron outputs for the four sources used in the present analysis are shown in Fig. 2.[9] The x-ray cross-sections for materials used here are shown in Fig 3.[10]

The local wavelength-dependent dose rate in the PMMA is then computed from the local transmitted power $p_{i,k}$ at a given position in the PMMA and the wavelength-dependent adsorption cross-section.

$$q_k = \rho \sigma_{a,k}\, p_{i,k} \tag{2}$$

The local total dose rate, dQ/dt, is then obtained by summing the wavelength-dependent doses over all photon energies,

$$\frac{dQ}{dt} = \sum_k q_k\, \delta E_k \tag{3}$$

where δE_k is one-half of the width of the band of photon energies between E_{k-1} and E_{k+1}. The units of this dose rate are energy per unit time per unit volume. For a constant synchrotron source, the total dose is therefore obtained simply by multiplying this total dose rate by the exposure time.

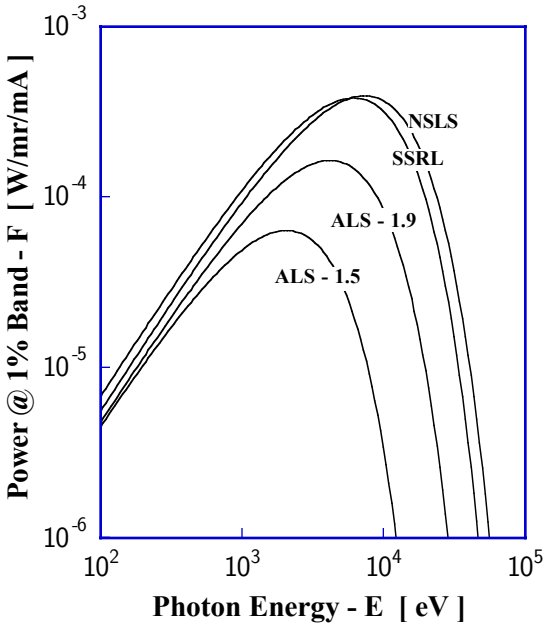

Figure 2. Synchrotron output for ALS (1.5 GeV, 4.8 m), ALS (1.9 GeV, 4.8 m), SSRL (3.0 GeV, 12.9 m) and NSLS (2.6 GeV, 6.9 m). Powers are those in a 1% band about the mean photon energy.

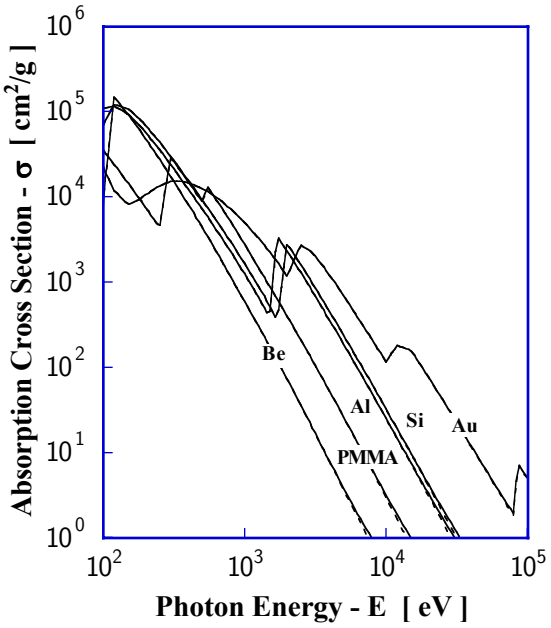

Figure 3. Absorption cross-sections for materials used in the present analysis. The PMMA cross-section is computed from its elemental constituents. Gold is used as the mask absorber in all results presented here.

This exposure model not only computes local total doses in the PMMA for a fixed set of filters, but also contains an iterative algorithm to adjust the thickness of a single selected filter in order to obtain a specified ratio of the top and bottom surface doses. As the filter thickness is increased, the x-ray spectrum shifts toward higher photon energies and so the profile of the dose through the PMMA thickness is flattened. This is because the remaining higher-energy photons encounter smaller absorption cross-sections within the PMMA, as shown in Fig. 3, so the incident power through the thickness is more uniform. By increasing the filter thickness, top-to-bottom dose ratios arbitrarily close to unity may thus be obtained, provided that the beam spectrum extends to sufficiently high energies. In contrast, a given source will provide some maximum dose ratio that cannot be exceeded. The value of this limit is determined by the unfiltered spectrum of the source. Adding filters to the beam can only increase the spectrum energy from this state and so can only reduce the dose ratio from the unfiltered limit. The model also performs a similar iterative adjustment of the mask absorber thickness. In this simpler case, the absorber thickness is adjusted to larger and smaller values until a specified surface or bottom dose in the masked region is obtained.

Dissolution rates during development generally depend on both the kinetics of the reaction and on the transport of PMMA fragments away from the dissolution surface. To account for both of these, we employ a composite function, c^*, that describes this simultaneous dissolution and fragment transport as two resistances in series. The resulting expression for the linear development rate (length per unit time) is

$$\frac{dy}{dt} = c^* U_0 \tag{4}$$

where y is the instantaneous location of the dissolution surface measured from the mold top, c^* is the solvent volume fraction at the dissolution surface, and U_0 is the kinetic-limited development rate at a specific dose and temperature. Given local values of c^* and U_0, Eq. 4 can be integrated numerically to yield the development distance as a function of time. The solvent volume fraction on the right side of Eq. 4 is given by

$$c^* = \frac{Sh\,D}{U_0\,y + Sh\,D} \tag{5}$$

where $Sh=ud/D$ is the average Sherwood number over the instantaneous feature height. The fragment diffusivity in the developer, D, can be approximated in terms of the monomer diffusivity, D_0~0.4x10^{-9} m^2/s, and development temperature, T,

$$D = D_0 \left(\frac{w_m}{w_e} \right)^2 \sqrt{\frac{T}{T_o}} \tag{6}$$

where T_0=293 K (20 C) is the reference temperature for D_0, w_m=100 g/mol is the monomer molecular weight of PMMA, and w_e is the molecular weight of the PMMA fragment.[11] The fragment molecular weight used here is based on an initial molecular weight of 3x10^6 g/mol and a fixed main-chain scission yield of 1.6 moles per 100 eV.[12]

The Sherwood number on the right of Eq. 5 is the ratio of the convective to diffusive rates of PMMA fragment transport. Its value depends on the magnitude of both forced and natural convection within a feature cavity, as well as the effective fragment diffusivity. Computing the Sherwood number requires knowledge of the entire flow field within the feature, so this is a very challenging task. However, a few bounding cases span many of the regimes relevant to LIGA.[8] First, even moderate forced convection over features having an aspect ratio below one-half will produce convective transport rates far in excess of those by diffusion alone. The Sherwood number in this limit becomes infinite, yielding the simple result c^*=1. Second, forced convection over a cavity is known to influence the local Sherwood number only in a region within about two or three cavity widths or diameters from the open end. Thus for feature aspect ratios above about four, the Sherwood number is usually unity indicating that fragment transport occurs by diffusion alone. The only exception to this guideline is when sonic agitation is employed. In this case, it appears that the development rate is not limited by diffusion even in features having aspect ratios that are very large, and so again c^*=1.

Because development rates at the PMMA surface are not subject to diffusion transport limitations, the lateral development rate can be computed using only the kinetic-limited rate. In differential form this is

$$\frac{dx}{dt} = U_0 \tag{7}$$

where x is the instantaneous lateral extent of sidewall dissolution and, in this case, the development rate U_0 is evaluated at the surface dose under the mask absorber. By integrating Eq. 7 over the time

interval required for development through the PMMA thickness, the maximum lateral extent of development, $\varepsilon=2x$, is obtained.

Kinetic-limited development rates normally depend on the development temperature and local total dose,[13] but may additionally depend on the dose rate and mean photon energy of the dose. In our general development model, the kinetic rate is computed from the PMMA molecular weight after the dose. This final molecular weight is computed from the initial molecular weight, a cross-linking yield, and a main-chain scission yield that depends on the mean photon energy of the absorbed dose. For simplicity, however, here we employ a kinetic-limited development rate that depends only on the total dose and development temperature. The form of this relationship is

$$U_0 = a\,\frac{(Q/b)^c}{1+(Q/b)^c}\,e^{-\frac{E_a}{R}\left(\frac{1}{T}-\frac{1}{T_r}\right)} \qquad \text{where} \qquad E_a = \frac{\alpha}{1+(Q/\beta)^\kappa} \tag{8}$$

and T_r=308 K (35 C) is a reference temperature. Parameters for the activation energy used here are α=139 kJ/mol, β=8.32 kJ/cm^3, and κ=2.38. The kinetic-limited development rates for GG developer at 35 C are shown in Fig. 4 along with the activation energy.[14]

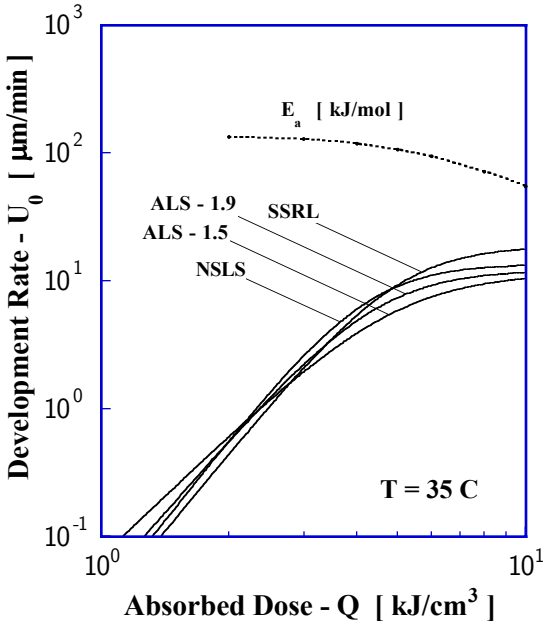

Figure 4. PMMA development rates at 35 C for GG developer as a function of absorbed dose. Coefficients for the sources are NSLS: a=13.5 μm/min, b=4.23 kJ/cm^3, c=4.21; SSRL: a=18.7 μm/min, b=5.03 kJ/cm^3, c=4.05; ALS-1.9: a=12.15 μm/min, b=4.47 kJ/cm^3, c=3.80; and ALS-1.5: a=11.5 μm/min, b=4.95 kJ/cm^3, c=3.20. The dashed line indicates the activation energy for kinetic-limited development.

SAMPLE RESULTS

As previously described, sidewall taper in a simplified view is just the ratio of the low-dose development rate in masked regions of the PMMA surface to the average development rate in unmasked regions over the entire mold thickness. This simplified view provides considerable insight into the phenomena influencing LIGA mold sidewall taper. First, and most obviously, a smaller thickness of the gold absorber will produce greater sidewall taper. A thinner mask yields a higher

dose in the masked region and so increases the lateral development rate without affecting the mean development rate through the thickness. Second, increased through-thickness dose variation will yield increased sidewall taper. This is because the masked-region development rate is fixed by the masked-region top dose, while the average through-thickness rate falls with increasing dose variation due to the lower development rates associated with lower doses deep in the PMMA. Third, increased development temperatures will yield greater sidewall taper. The reason for this is that the activation energy of the kinetic-limited development rate is dose dependent and is larger at lower doses. Increased temperatures therefore increase low-dose development rates relative to high-dose rates. Fourth, features having larger aspect ratios will exhibit increased sidewall taper. Development rates deep in high aspect-ratio features often are not limited by dissolution kinetics, but instead are limited by the diffusive transport of PMMA fragments to the mold surface. High aspect-ratio features will therefore develop more slowly, giving an average through-thickness rate that is lower. Lateral sidewall development rates at the mold surface are, of course, not subject to this additional transport limitation. Finally, very high doses in the unmasked region will likely increase sidewall taper. The development rates at very high doses asymptote to a constant value, so the ratio of development rates in the masked and unmasked regions increases toward unity as the dose increases without bound.

To help quantify these general observations, we have made sample calculations of the minimum absorber thickness yielding a prescribed sidewall taper over a wide range of required tolerances and exposure and development conditions. The first of these is illustrated in Fig. 5 for exposure at the ALS synchrotron operating at 1.9 GeV. Here, and in all subsequent cases employing this baseline source, the beam is filtered by a 127 μm beryllium window and a 100 μm silicon mask substrate. In this figure, the computed minimum thickness of the gold absorber, the development time, top surface dose and dose in the masked regions are shown as a function of the absorbed bottom dose for a range of values of the sidewall dissolution distance. The development temperature is 35 C in each case. We see that the minimum absorber thickness increases smoothly with decreasing allowable sidewall dissolution. Over the range of values shown, the absorber thickness increases between 20 and 30% for each decade reduction in allowable sidewall taper. At ε=10 μm and a bottom dose of 4 kJ/cm^3 the minimum absorber thickness is 5.5 μm; at ε=0.1 μm and the same dose this minimum thickness increases to 9.7 μm. As expected, we also see that increasing the dose requires increasing the absorber thickness in order to maintain the same sidewall dissolution. At ε=1 μm and a bottom dose of 1 kJ/cm^3 the minimum absorber thickness is 6.8 μm; at the same tolerance and a bottom dose of 10 kJ/cm^3, this minimum thickness increases to 10.4 μm. Indeed, at all tolerance levels a bottom dose of 10 kJ/cm^3 yields a minimum absorber thickness that is about 50% greater than that at 1 kJ/cm^3. Note that here the development time and PMMA top surface dose are not altered by changes in the prescribed sidewall tolerance or absorber thickness. This is because the source, beam filters, feature size and PMMA thickness are all fixed in these calculations, and these are the only parameters affecting the top dose and development history.

The results shown in Fig. 5 indicate that decreasing the bottom dose always decreases the minimum absorber thickness, and so there exists no optimum bottom dose for which the absorber thickness is minimized. The practical limit of this is that the development time becomes prohibitively large as the bottom dose becomes small. At a bottom dose of 1 kJ/cm^3, the computed development time is about

150 hrs – nearly a week! At all doses above about 4 kJ/cm^3, however, the development time remains relatively flat, so bottom doses above this level provide little benefit but do further increase the minimum absorber thickness. Thus a bottom dose of 3 to 5 kJ/cm^3 seems to a practical optimum, at least for this case.

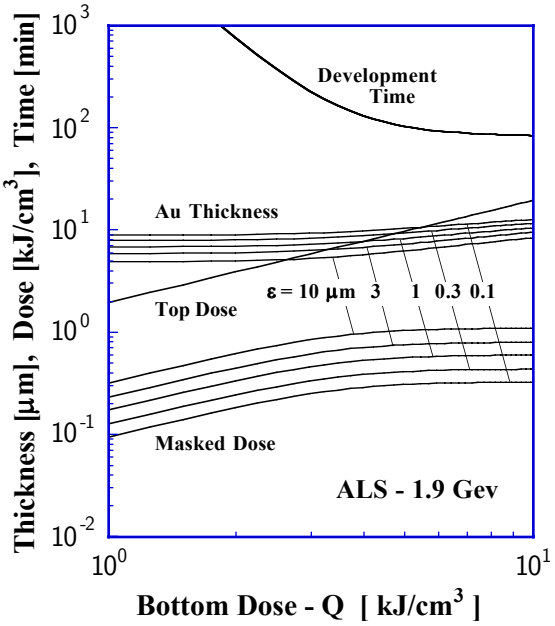

Figure 5. Minimum mask absorber thickness increases by 20 to 30% for each order-of-magnitude reduction in sidewall taper. Low doses require the smallest absorber thickness. Conditions: T=35 C; h=1 mm; d=10 mm.

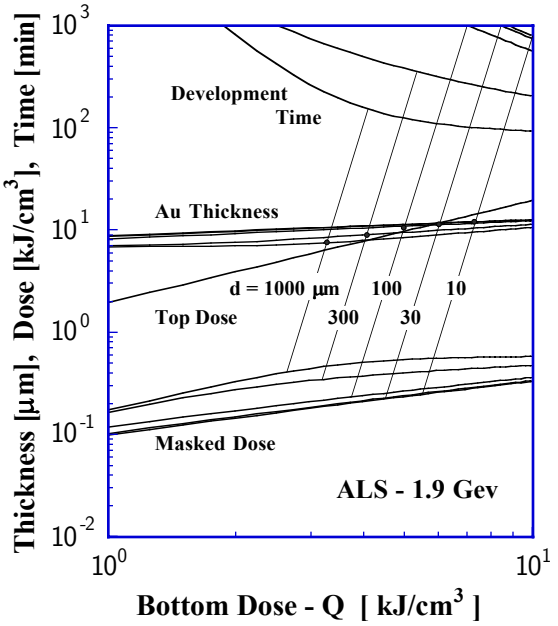

Figure 6. Longer development times for very small features increase the minimum absorber thickness by at most about 40% for a 1 mm PMMA thickness. Conditions: T=35 C; h=1 mm; ε=1 µm.

Figure 6 shows similar results for calculations of the minimum absorber thickness, though in this case the parameter varied is the feature size, d, while the extent of sidewall dissolution is held constant at ε=1 µm. Here we see that the development time increases significantly as the feature size is reduced due to diffusion transport limitations, even though the dose profiles through the PMMA thickness are the same in each instance. This increased development time necessitates a larger absorber thickness for smaller feature sizes: at a bottom dose of 4 kJ/cm^3, the computed minimum absorber thickness for a 1 mm feature is only 7.9 µm, while that for a 10 µm feature is 11.0 µm. Since most LIGA molds contain features of widely varying size, the minimum absorber thickness will thus usually be determined by tolerances on the smallest features present.

In Fig. 6 we also see that development times exhibit two limiting behaviors in the extremes of very large and very small features. The first is the kinetic limit for large features, which exhibits a strong dependence on the local absorbed dose, but no dependence on feature size. Note that development times at a fixed bottom dose are nearly the same for a 10 mm feature (Fig. 5) and a 1 mm feature (Fig. 6). This is the limit of an infinite Sherwood number. The second limiting behavior occurs in very small features, for which the development rate is controlled by PMMA fragment diffusion

within the feature cavity. In this case, the development time grows as the square of the PMMA thickness, but again shows no dependence on feature size since the cross-section area for diffusive transport equals the area of dissolution at any feature size. This is the limit of a Sherwood number of unity, which applies to any feature of aspect ratio greater than about four. Such behavior is illustrated in Fig. 6 by the similar development times of the 10 and 30 μm features.

These limiting behaviors in the development time give rise to corresponding limits in the minimum absorber thickness and associated dose in masked regions of the PMMA. The minimum absorber thickness for small feature sizes is 20 to 40% greater than that for large feature sizes. The maximum difference between these occurs near a bottom dose of 4 kJ/cm^3, and the influence of feature size on minimum absorber thickness is reduced at both higher and lower doses. As before, the variation of minimum thickness with dose is an increase of about 40 to 50% between bottom doses of 1 and 10 kJ/cm^3, independent in this case of the feature size.

Diffusion-limited development rates in high aspect-ratio features cannot be enhanced significantly by forced convection across the mold top.[8] Such forced convection produces a series of closed convective cells within the mold cavity. The speeds in these cells decay exponentially with depth from the mold top and become negligible within two to three feature widths into the cavity. The role of natural convection in the development process has not yet been studied, though it is unlikely that this will produce significant benefits owing to the large viscosity of the polymer-laden developer. The only promising means to increase diffusion-limited development rates now appears to be ultrasonic or megasonic agitation.[7] Based on a very few observations, the primary benefit of sonic agitation appears to be increased rates of PMMA fragment transport, and as such even very small features developed using this method seem to exhibit kinetic-limited development histories. Sonic agitation should therefore permit a 30 to 40% reduction in absorber thickness for small features having large aspect ratios.

We next consider the effect of the synchrotron spectrum on minimum absorber thickness. One might believe, *a priori*, that a more energetic spectrum would require a larger absorber thickness. As shown in Fig. 7, however, this does not appear to be the case, at least over the range of sources considered here. Figure 7 shows the computed minimum absorber thickness for exposure at the SSRL, NSLS and ALS synchrotrons. For each source the beam is filtered by a thin beryllium window and a 100 μm silicon mask substrate. Given a fixed sidewall dissolution distance of ε=1 μm, we see that the minimum absorber thickness is essentially independent of the source spectrum. Although the through-thickness dose profiles, development times and the masked doses all vary significantly from one source to another, the minimum absorber thickness remains essentially unaffected. The reason for this unexpected result lies in part in the absorption cross-section of PMMA. For a 1 mm PMMA thickness, only those photons encountering an absorption cross-section between about 1 and 10^4 cm^2/g contribute significantly to the absorbed dose. From Fig. 3, this limits the useful range of photon energies to between about 1 and 10 keV. More energetic photons pass through the thickness without interaction, while those of lesser energies are absorbed in the filters or in a very thin layer near the PMMA surface. Because all of the synchrotron spectra are fairly flat in this range, and further the ratio of the gold and PMMA cross-sections is fairly uniform in this range, the

ratio of minimum absorber thickness to the PMMA thickness is nearly constant across these sources.

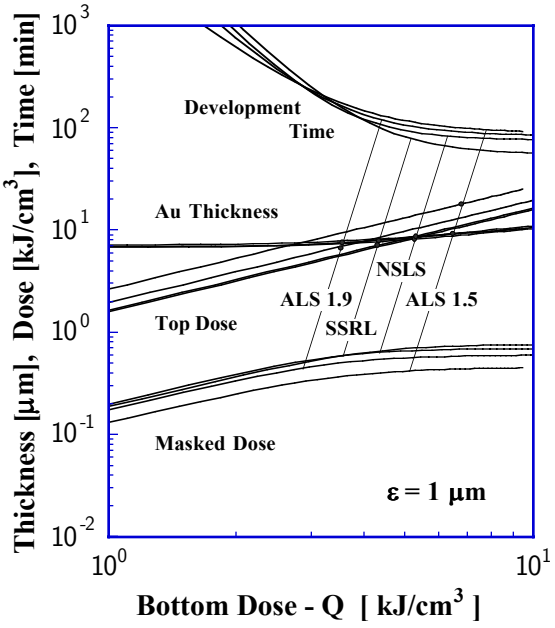

Figure 7. The synchrotron sources used by Sandia require very similar gold absorber thickness to produce any prescribed sidewall taper. Conditions: T=35 C; h=1 mm; d=10 mm; ε=1 μm.

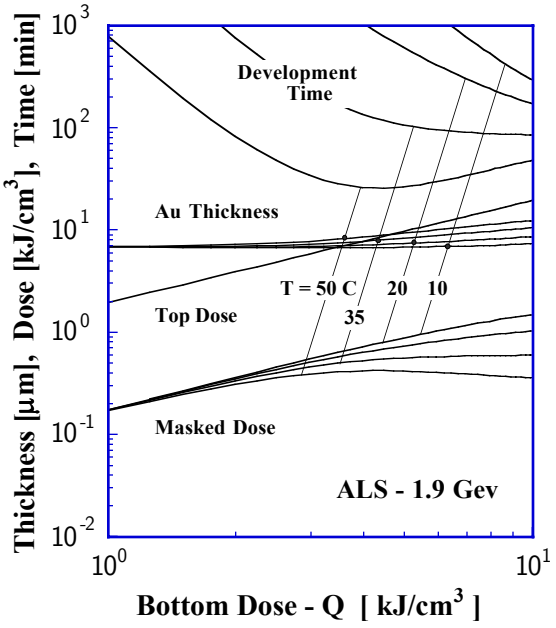

Figure 8. Increased development temperature requires a larger absorber thickness at high doses due to dose dependence of the dissolution rate activation energy. Conditions: T=35 C; h=1 mm; d=10 mm; ε=1 μm.

As discussed above, increased development temperatures are likely to increase the minimum absorber thickness for any prescribed sidewall taper. This is illustrated in Fig. 8 for an ALS exposure at 1.9 GeV and an allowable sidewall dissolution distance of ε=1 μm. Here we see that the effect of development temperature is influenced by the magnitude of the dose. At low doses the minimum absorber thickness is independent of the temperature, despite orders-of-magnitude variation in development times. At large bottom doses the required absorber thickness increases with increasing temperature. At a bottom dose of 10 kJ/cm^3, the minimum absorber thickness increases from 7.2 μm at a temperature of 10 C to 12.3 μm at 50 C. Thus over the full practical range of bottom dose and development temperature, increased temperatures increase the minimum absorber thickness by about 70%. At bottom doses below 4 kJ/cm^3, the effect of temperature on absorber thickness is limited to about 13%. The origin of this dose-dependent behavior is that activation energy approaches a constant at very low doses (see Fig. 4). At low doses, the ratio of the development rates in the masked and unmasked regions is therefore independent of temperature and instead depends only on the absorber thickness. At large bottom doses, in contrast, the activation energy corresponding to doses in the masked and unmasked areas differ significantly. Because the activation energy falls with increasing dose, larger development temperatures require a larger absorber thickness to compensate for the relatively reduced development rates in the high-dose PMMA. Note that the unusual shape of the development time curve at 50 C is a result of the form

of the dissolution kinetics given by Eq. 8. Here the development rate at very high temperatures actually decreases with increasing dose due to the dose-dependent decline of the activation energy. However, a temperature of 50 C is just outside the range of the data used to construct Eq. 8, so it is not clear whether this behavior is real or is merely an artifact of extrapolating outside the applicable range of the fit. Probably, it is the latter. In either case, the conclusions reached above are not much affected.

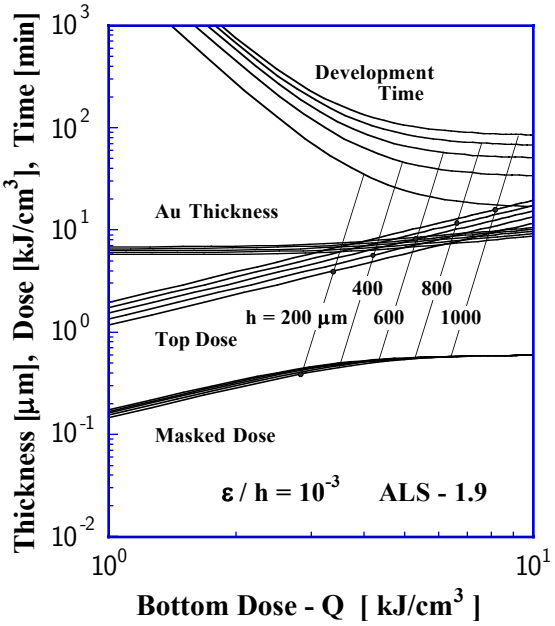

Figure 9. Minimum absorber thickness is insensitive to PMMA thickness for a fixed sidewall taper, ε/h, but increases with thickness for a fixed sidewall dissolution distance, ε. Conditions: T=35 C; d=10 mm; ε/h =10^{-3}.

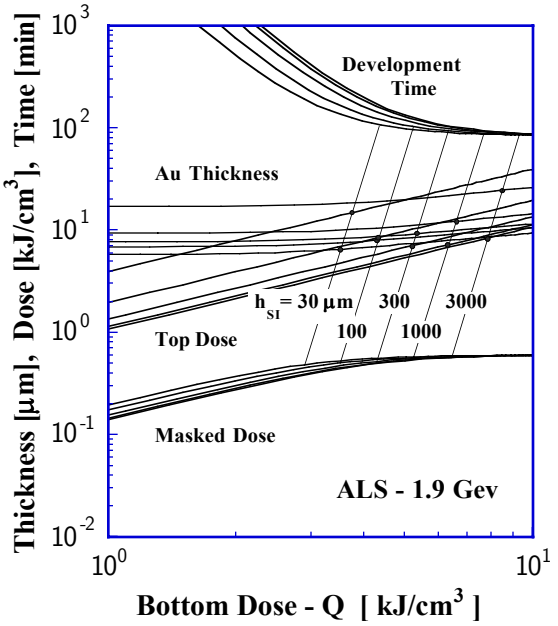

Figure 10. A very thick silicon mask substrate leads to excessive beam filtering and dramatically increases the minimum absorber thickness. Conditions: T=35 C; d=10 mm; ε=1 µm.

We now consider the influence of PMMA thickness on minimum absorber thickness. Figure 9 shows computed absorber thickness, development times and bottom doses for cases in which the prescribed sidewall dissolution distance is scaled by the PMMA thickness such that the sidewall taper is fixed at ε/h=10^{-3}. Here we see that the range of minimum absorber thickness at any given dose is weakly dependent of PMMA thickness and spans only about 20% for all PMMA thickness between 200 and 1000 µm. The reason for this is simply that the total development time for a given bottom dose is roughly proportional to the PMMA thickness. Thus the sidewall dissolution distance is also roughly proportional to the PMMA thickness when masked doses are equal, and this occurs at roughly a fixed absorber thickness for any fixed bottom dose. This linear scaling should also hold as the prescribed sidewall taper is increased or reduced, so the rule of thumb from Fig. 5 should still apply: each order-of-magnitude increase or decrease in the prescribed sidewall taper corresponds to a 20 to 30% decrease or increase in the minimum absorber thickness.

Our final sample calculation addresses the effects of beam filters on the minimum absorber thickness. Here we limit our attention to the influence of the silicon mask substrate and the effect of its thickness on absorber thickness. Figure 10 shows computed minimum absorber thickness for substrate thickness in the range from 30 to 3000 μm. We see that the substrate thickness has a significant influence over its entire range, but this influence is especially pronounced when the thickness grows very large. As the substrate thickness increases from 30 to 1000 μm, the minimum absorber thickness increases from 6.5 to 10.0 μm at a bottom dose of 4 kJ/cm^3. In this range, a thirty-fold increase in substrate thickness yields about a 60% increase in the required absorber thickness. Between 1000 and 3000 μm, however, the absorber thickness increases to 18.0 μm. Thus in this range, a three-fold increase in substrate thickness nearly doubles the minimum absorber thickness. This occurs because the silicon substrate strongly shifts the beam spectrum in the region of importance for LIGA exposures, 1 to 10 keV, only when its thickness is very large. We therefore conclude that minimizing the mask substrate thickness is important to minimizing absorber thickness, even for synchrotron sources of relatively high beam energy, and that the use of other beam filters should be avoided unless necessary to achieve acceptable top-to-bottom ratios of the absorbed dose.

SUMMARY

To help optimize mask design and exposure and development conditions for the LIGA process, we have developed numerical models describing both x-ray exposure of the PMMA resist and development of the exposed part. The exposure model addresses multi-wavelength, one-dimensional x-ray transmission and absorption through multiple beam filters, the mask absorber and substrate, and the PMMA resist. The development model describes the one-dimensional evolution of the dissolution front, taking into account the local absorbed dose through the PMMA thickness. Local dissolution rates are computed from phenomenological relations based on measured kinetic-limited development rates and a quasi-empirical expression accounting for advective and diffusive transport of PMMA fragments from the dissolution surface to the open mold top. The development model additionally includes an auxiliary equation describing the lateral sidewall development rate. This equation is integrated in time over the period of development to yield the extent of sidewall dissolution.

These coupled models were used to investigate the minimum thickness of the mask absorber required to provide a prescribed allowable sidewall taper. Although many factors also influence sidewall taper, this is the primary consideration in determining a minimum acceptable absorber thickness. Here we have made sample calculations of the minimum absorber thickness as a function of the PMMA absorbed bottom dose for a range of values of the allowable sidewall taper, feature size, development temperature, PMMA thickness and the thickness of the silicon mask substrate. In addition, we have examined the influence on minimum absorber thickness of several x-ray sources: SSRL; NSLS; and ALS operating at 1.5 and 1.9 GeV.

We find that the minimum absorber thickness depends rather weakly on all of the parameters examined here. Each decade reduction in the prescribed sidewall taper requires a 20 to 30% increase in absorber thickness. Small features sizes, without sonic agitation, require an absorber thickness at

most about 40% greater than that needed for features of aspect ratio less than about three. The minimum absorber thickness for any fixed sidewall taper is nearly independent of PMMA thickness over the range from 200 to 1000 μm. As anticipated, the minimum absorber thickness increases with increasing absorbed dose and increasing development temperature. For the former, minimum absorber thickness increases about 50% as the absorbed bottom dose increases from 1 to 10 kJ/cm^3. For the latter, increasing the development temperature from 10 to 50 C increases the minimum absorber thickness about 70% at high bottom doses, but has little effect at all bottom doses below about 3 kJ/cm^3. Lastly, increasing the mask substrate thickness from 30 to 1000 μm increases the minimum absorber thickness by about 60%. Between 1000 and 3000 μm, however, the effect of substrate thickness is very strong and increases the absorber thickness by about a factor of two. While each of these effects is relatively small, their unfavorable combination may double or triple the minimum absorber thickness needed to achieve some desired sidewall taper.

Based on these observations, a 14 μm gold absorber on a 100 μm silicon substrate should provide a sidewall taper better than 10^{-3} for all of the sources considered here and for the full practical range of feature size, development temperature and PMMA dose. Similarly, an 18 μm gold absorber should provide a sidewall taper of better than 10^{-4}. By limiting the bottom dose to less than 4 kJ/cm^3, the development temperature to less than 35 C, and by using sonic agitation during development, the minimum absorber thickness may be reduced to 8 and 10 μm for sidewall tapers of 10^{-3} and 10^{-4}, respectively. To realize these objectives of course requires that all other factors influencing sidewall taper are also controlled within acceptable limits, but increasing the absorber thickness above these values should not be necessary.

Finally, the minimum absorber thickness computed here is quite sensitive to the kinetic-limited development rates at very low doses. The low-dose rates used here are simple power-law extensions of the development rates measured for doses in the range of 1 to 2 kJ/cm^3. It is well known that some types of cross-linked PMMA exhibit an abrupt threshold below which measurable dissolution ceases. Such behavior will reduce the minimum absorber thickness in all cases presented here. In contrast, linear PMMA may show a finite limiting value of the development rate even at very low doses. In this case, the minimum absorber thickness will increase. This latter behavior also disfavors low absorbed doses in unmasked PMMA, giving rise to a true minimum absorber thickness and optimum bottom dose.

ACKNOWLEDGMENT

Development of the LEX-D code was funded in part by a Sandia LDRD and in part by the Sandia Materials Science Research Foundation. The present study was funded by the Sandia Revolution in Engineering Program. Sandia is a multiprogram laboratory operated by Sandia Corporation, a Lockheed Martin Company, for the United States Department of Energy under contract DE-AC04-94AL85000.

REFERENCES

1. E. W. Becker, W. Ehrfeld, P. Hagmann, A. Maner, D. Munchmeyer, "Fabrication of Microstructures with High Aspect Ratios and Great Structural Heights by Synchrotron Radiation Lithography, Galvanoforming and Plastic Moulding (LIGA Process)," *Microelectronic Eng.* **4**, pp. 35-56, 1986.
2. D. Munchmeyer and W. Ehrfeld, "Accuracy Limits and Potential Applications of the LIGA Technique in Integrated Optics," Proceedings of the SPIE*, Micromachining of Elements with Optical and other Submicrometer Dimensional and Surface Specification* **803**, pp. 72-79, 1987.
3. G. Freiertag, W. Ehrfeld, H. Lehr, A. Schmidt and M. Schmidt, "Calculation and Experimental Determination of the Structure Transfer Accuracy in Deep X-Ray Lithography," *J. Micromech. Microeng.* **7**, No 4, pp. 323-331, 1998.
4. H. Zumaque, G. A. Kohring and J. Hormes, "Simulation Studies of Energy Deposition and Secondary Processes in Deep X-Ray Lithography," *J. Micromech. Microeng.* **7**, No. 2, pp. 79-88, 1998.
5. J. Klein, H. Guckel, D. P. Siddons and E. D. Johnson, "X-Ray Masks for Very Deep X-Ray Lithography," *Microsystem Technologies* **4**, pp. 70-73, 1998.
6. Z. Liu, F. Bouamrane, R. K. Kupka, A Labeque and S. Megtert, "Resist Dissolution Rate and Inclined-Wall Structures in Deep X-Ray Lithography," *J. Micromech. Microeng.* **8**, No 4, pp. 293-300, 1998.
7. J. Zanghellini, S. Achenbach, A. El-Kholi, J. Mohr, and F. J. Pantenburg, "New Development Strategies for High Aspect Ratio Microstructures," *Microsystem Technologies* **4**, pp. 94-97, 1998.
8. S. K. Griffiths, R. H. Nilson, R. W. Bradshaw, A. Ting, W. D. Bonivert, J. T. Hachman and J. M. Hruby, "Transport Limitations in Electrodeposition for LIGA Microdevice Fabrication," Proceedings of the SPIE, *Micromachining and Microfabrication Process Technology* IV **3511**, pp. 364-375, 1998.
9. Ernst-Eckhard Koch, Ed., *Handbook of Synchrotron Radiation*, Vol. 1A, North-Holland Publishing Company, 1983.
10. F. Biggs and R. E. Lighthill, "Analytical Approximations for X-Ray Cross Sections," SAND87-0070, Sandia National Laboratories Report, August 1988.
11. J. S. Kirkaldy and D. Y. Young, *Diffusion in the Condensed State,* The Universities Press, Belfast, 1987.
12. R. L. Clough and S. W. Shalaby, Eds., *Irradiation of Polymers - Fundamentals and Technological Applications*, American Chemical Society, Washington, DC, 1996.
13. O. Schmalz, M. Hess and R. Kosfeld, "Structural Changes in Poly(Methyl Methacrylate) During Deep-Etch X-Ray Synchrotron Radiation Lithography," Parts I, II, III, *Die Angewandte Makromolekulare Chemie* **239**, pp. 63-106, 1996.
14. M. X. Tan, M. A. Bankert, S. K. Griffiths, A. Ting, D. R. Boehme, S. Wilson and L. M. Balser, "PMMA Dose Studies at Various Synchrotron Sources and Exposure/Development Conditions," Proceedings of the SPIE*, Materials and Device Characterization in Micromachining* **3512**, 1998.

UNLIMITED RELEASE
INITIAL DISTRIBUTION

Dean Wiberg
NASA Jet Propulsion Laboratory
Microdevices Division
4800 Oak Grove Drive
MS 302-231
Pasadena, CA 91109-8099

Keith Jackson
Lawrence Berkely National Laboratory
Center for X-Ray Optics
Berkeley, CA 944720

Chantel Khan Malek
CAMD
3990 W. Lakeshore Drive
Baton Rouge, LA 70803

Klaus F. Jensen
Massachusetts Institute of Technology
Building 6-469
Chemical Engineering
Cambridge, MA 02139

1434 G. E. Pike, 1802
1411 D. B. Dimos, 1831
0481 K. D. Meeks, 2167
Attn: B. A. Potts, 2168
0329 D. W. Plummer, 2643
Attn: T. R. Christenson, 2643
A. D. Oliver, 2643
E. J. Garcia, 2643
9003 D. L. Crawford, 5200
Attn: J. E. Costa, 5203
9006 D. J. Havlik, 5201
1223 P. J. Wilson, 5202
9001 T. O. Hunter, 8000
Attn: M. E. John, 8100
R. C. Wayne, 8400
9420 L. A. West, 8200
Attn: G. D. Kubiak, 8250
9403 M. A. Bankert, 8230
9403 D. R. Boehme, 8230
9403 W. D. Bonivert, 8230
9403 D. A. Chinn, 8230
9403 J. T. Hachman, 8230
9403 J. M. Hruby, 8230 (5)
9403 A. M. Morales, 8230
9403 S. D. Leith, 8230
9403 M. X. Tan, 8230
9403 P. M. Dentinger, 8250
9054 W. J. McLean, 8300
Attn: W. Bauer, 8358
D. R. Hardesty, 8361
L. A. Rahn, 8351
F. P. Tully, 8353
R. W. Carling, 8362
9041 J. S. Binkley, 8345
9042 S. K. Griffiths, 8345 (5)
9042 A. Ting, 8345 (5)
9042 R. H. Nilson, 8345
9405 T. M. Dyer, 8700
Attn: C. M. Hartwig, 8701
M. I. Baskes, 8712
J. C. F. Wang, 8713
G. J. Thomas, 8715
K. L. Wilson, 8716
S. M. Foiles, 8717
9003 D. L. Lindner, 8902
0841 P. J. Hommert, 9100

9018 Central Technical Files, 8940-2 (3)
0899 Technical Library, 4916 (4)
9021 Technical Communications Dept., 8815
Technical Library, MS 0899, 4916
9021 Technical Communications Dept., 8815
for DOE/OSTI, 8815 (2)